PTP1B regulates non-mitochondrial oxygen consumption via RNF213 to promote tumour survival during hypoxia

Robert S. Banh[1,2], **Caterina Iorio**[#2], **Richard Marcotte**[#2], **Yang Xu**[#1,2], **Dan Cojocari**[1,2], **Anas Abdel Rahman**[3,4], **Judy Pawling**[3], **Wei Zhang**[5], **Ankit Sinha**[1,2], **Christopher M. Rose**[6], **Marta Isasa**[6], **Shuang Zhang**[7], **Ronald Wu**[1,2], **Carl Virtanen**[2], **Toshiaki Hitomi**[8], **Toshiyuki Habu**[9], **Sachdev S. Sidhu**[5], **Akio Koizumi**[8], **Sarah E. Wilkins**[10], **Thomas Kislinger**[1,2], **Steven P. Gygi**[6], **Christopher J. Schofield**[10], **James W. Dennis**[3], **Bradly G. Wouters**[1,2], and **Benjamin G. Neel**[2,7]

[1]Department of Medical Biophysics, University of Toronto, Toronto, ON, M5G 2M9, Canada

[2]Princess Margaret Cancer Centre, University Health Network, Toronto, ON, M5G 1L7, Canada

[3]Lunenfeld-Tanenbaum Research Institute, Mount Sinai Hospital, Toronto, ON, M5G 1X5, Canada

[4]Department of Genetics, Research Center, King Faisal Specialist Hospital and Research Center, Riyadh, Saudi Arabia

[5]Donnelly Centre for Cellular and Biomolecular Research, Banting and Best Department of Medical Research, University of Toronto, Toronto, ON, M5S 3E1, Canada

[6]Department of Cell Biology, Harvard Medical School, Boston, Massachusetts 02115, USA

[7]Laura and Isaac Perlmutter Cancer Center, New York University Langone Medical Center, New York University, New York, NY 10016, USA

[8]Department of Health and Environmental Sciences, Graduate School of Medicine, Kyoto University, Kyoto, Japan

[9]Department of Radiation System Biology, Institute of Radiation Biology Center, Kyoto University, Kyoto, Japan

[10]Chemistry Research Laboratory, Oxford University, 12 Mansfield Road, Oxford OX1 3TA, UK

Correspondence should be addressed to B.G.N.

[#] These authors contributed equally to this work.

Abstract

Tumours exist in a hypoxic microenvironment and must limit excessive oxygen consumption. Hypoxia-inducible factor controls mitochondrial oxygen consumption, but how/if tumours regulate non-mitochondrial oxygen consumption (NMOC) is unknown. Protein-Tyrosine Phosphatase-1B (PTP1B) is required for *Her2/Neu*-driven breast cancer (BC) in mice, though the underlying mechanism and human relevance remain unclear. We found that PTP1B-deficient *HER2$^+$* xenografts have increased hypoxia, necrosis and impaired growth. *In vitro*, PTP1B deficiency sensitizes *HER2$^+$* BC lines to hypoxia by increasing NMOC by α-KG-dependent dioxygenases (α-KGDDs). The Moyamoya disease gene product RNF213 , an E3 ligase, is negatively regulated by PTP1B in *HER2$^+$* BC cells. *RNF213* knockdown reverses the effects of PTP1B-deficiency on α-KGDDs, NMOC and hypoxia-induced death of *HER2$^+$* BC cells, and partially restores tumourigenicity. We conclude that PTP1B acts via RNF213 to suppress α-KGDD activity and NMOC. This PTP1B/RNF213/α-KGDD pathway is critical for survival of *HER2$^+$* BC, and possibly other malignancies, in the hypoxic tumour microenvironment.

Many, if not most, solid tumours contain significant areas of hypoxia or anoxia1. Cells activate three major adaptive pathways in response to oxygen deficit, which together function to limit O_2 consumption and maintain energy balance/metabolism2. In response to even mild hypoxia, the transcription factor HIF1α becomes stabilized. HIF1α directs the expression of multiple genes, which promote neo-vascularization, suppress protein synthesis, increase glycolysis and decrease mitochondrial O_2 consumption. More severe hypoxia activates AMPK, which suppresses mTOR and limits excess energy consumption from the synthesis of protein, lipid and other macromolecules3,4. Severe hypoxia also causes endoplasmic (ER) stress and activates the unfolded protein response (UPR). The UPR activates three distinct ER sensors for unfolded proteins, PERK, IRE1 and ATF65. Together, they impede translation and induce the expression of genes for protein refolding and ER redox balance. Although mitochondria are responsible for the vast majority of cellular oxygen consumption, a number of biological processes, including, but not limited to, protein folding, lipid and collagen synthesis, and DNA and histone demethylation, involve reactions that utilize oxygen directly. Whether (and how) non-mitochondrial oxygen consumption (NMOC) is regulated during oxygen deprivation is unknown.

Mammals have a large family of genes (>60) encoding "α-KG (α-ketoglutarate)-dependent dioxygenases (α-KGDDs)", which use α-KG and O_2 as co-substrates to catalyze hydroxylation and demethylation reactions6–9. These enzymes require Fe^{+2} and typically, ascorbate (Vitamin C), which functions to maintain the oxidation state of the Fe residue7–10. Examples of α-KGDDs include the HIF prolyl hydroxylases (PHD1-3), which direct HIF ubiquitylation and are critical for its regulation by O_2, the FIH asparaginyl hydroxylase, which regulates HIF association with P300, TET family DNA demethylases, the Jumanji histone demethylases, the collagen hydroxylases and a key enzyme in carnitine metabolism, γ-butyrobetaine hydroxylase (BBOX).

The protein-tyrosine phosphatase PTP1B, encoded by *PTPN1*, is best known as an essential regulator of insulin and leptin receptor signaling; accordingly, *Ptpn1*^{-/-} mice are hypersensitive to insulin, lean and resistant to high fat diet-induced obesity[11–13]. PTP1B also has been implicated as a negative regulator of several other receptor-tyrosine kinases (RTKs), and is suggested to regulate pyruvate kinase M2 and PERK[14–16]. Surprisingly, however, *PTPN1* is amplified (~5%) and overexpressed (~72%) in many breast tumours[17,18], and several years ago, we and others reported that mouse *Ptpn1* is required for efficient mammary tumourigenesis by *Her2/Neu*[19,20]. Furthermore, mammary-specific over-expression of PTP1B causes breast tumours[20]. The underlying mechanism of the pro-oncogenic effects of PTP1B has remained unclear/controversial[19,20], however, as has its role in human *HER2+* breast cancer.

Moyamoya disease is a rare disorder (incidence ~1:100,000)[21] that occurs in sporadic and inherited forms. Characterized by vascular occlusions, usually affecting the circle of Willis, it typically presents in adolescents or young adults. The inherited form is strongly associated with single nucleotide polymorphisms (SNPs) in *RNF213*, which encodes a large protein (591kDa) containing AAA+ ATPase and E3 ligase domains. Up to 1% of the Japanese (and other Asian) population have the causative SNP, suggesting that important environmental contributors and/or genetic modifiers must exist.

In studying the effects of PTP1B deficiency on *HER2+* breast cancer (BC) lines, we found that PTP1B is essential for their response to severe hypoxia *in vitro* and *in vivo*. Further analysis uncovered a previously unreported pathway involving PTP1B, RNF213, and αKGDDs. Hence, our results reveal unexpected connections between tyrosine phosphorylation, Moyamoya disease, αKGDDs and the regulation of NMOC in the tumour microenvironment.

Results

PTP1B is required for tumourigenicity of *HER2+* BC cells

To explore its potential role in human *HER2+* BC, we depleted PTP1B from several *HER2+* breast cancer (BC) lines by stably expressing *PTPN1* shRNA (Supplementary Fig. 1a). PTP1B-deficiency did not affect cell proliferation in normal media (10% serum), low serum (1% serum), low density, low glucose (0.5g/L) or in the absence of glutamine (Supplementary Fig. 1b,c). PTP1B deficiency also had no consistent effect on signalling in response to growth factor signalling, as assessed by pSTAT3, pAKT and pERK levels (Supplementary Fig. 1d). Nor did PTP1B-deficiency attenuate colony formation in soft-agar or Matrigel; in fact, for some lines, lack of PTP1B resulted in increased colony size (Supplementary Fig. 1e, f). Hence, we conclude that PTP1B is not required for proliferation of *HER2+* BC cells *in vitro*.

Ptpn1-deficiency delays the onset of breast tumours and prolongs the survival of *MMTV-Neu[NT]* mice (Ref. 19, 20; also see Supplementary Fig. 2a), so we investigated the role of PTP1B in tumour initiation by human *HER2+* BC cell lines. In marked contrast to its lack of effects *in vitro*, but consistent with the effects of an allosteric PTP1B inhibitor[22], *PTPN1*-KD inhibited *HER2+* tumour growth (Fig. 1a). Re-expressing wild-type (WT) mouse PTP1B

(m1B) in 1B-KD cells by using a *Ptpn1* cDNA (which is *PTPN1* shRNA-resistant) rescued tumour growth. By contrast, the catalytically impaired R221M mutant (m1B-RM) could not restore tumourigenicity (Fig. 1b). Therefore, the anti-tumourigenic effects of the *PTPN1* shRNA are "on-target", and PTP1B catalytic activity is required for its pro-tumourigenic effects. PTP1B expression also was required for tumour maintenance, as shown by experiments using an IPTG-inducible *PTPN1 shRNA* (i1B-KD) expressed in BT474 cells (Fig. 1c). Despite the marked effect of PTP1B-deficiency on tumour growth, there were no consistent differences in MEK, ERK, AKT or S6 phosphorylation in parental vs. PTP1B-deficient tumours (Supplementary Fig. 3a). Consistent with a mouse model23, immunohistochemical analysis showed no consistent difference in proliferation (BrdU incorporation/Ki67) or angiogenesis (CD31) as a consequence of PTP1B deficiency (Supplementary Fig. 3b-d).

PTP1B deficiency/inhibition sensitizes HER2⁺ BC cells to hypoxic cell death

PTP1B-deficient *HER2⁺* tumours, although substantially smaller, were more necrotic (Fig. 1d; red arrows) and more hypoxic, as shown by EF5 immunostaining (Fig. 1d, e and Supplementary Fig. 3e). Inducing *PTPN1*-shRNA expression after tumours had started to form resulted in markedly increased EF5 reactivity (Fig. 1f, g and Supplementary Fig. 3f), indicating that increased hypoxia was an acute effect of PTP1B depletion, rather than a response to sustained PTP1B deficiency. Similar effects were observed in a mouse model: although nine month-old *Ptpn1⁻/⁻*; *MMTV-Neu^{NT}* and *Ptpn1⁺/⁺*; *MMTV-Neu^{NT}* mice had comparable numbers of hyperplastic lesions, in PTP1B-deficient animals, these lesions displayed more EF5 staining (Supplementary Fig. 2b-d). Hence, we conclude that PTP1B controls *HER2⁺* tumour hypoxia and survival.

Next, we assessed the effect of PTP1B-deficiency on *HER2⁺* BC cells exposed to hypoxia *in vitro*. *PTPN1*-KD decreased the survival of multiple *HER2⁺* lines in bulk culture (Fig. 2a) and in clonogenic assays (Fig. 2b) following exposure to 0.1% or 0.2% O_2, respectively. Importantly, expressing WT m1B, but not m1B-RM, rescued hypoxia-induced cell death in 1B-KD cells (Fig. 2c). Conversely, treatment with a specific PTP1B inhibitor24 induced cell death in parental *HER2⁺* BC cells exposed to hypoxia, but had no effect in normoxia, indicating that the protective effect of PTP1B in hypoxia is phosphatase activity-dependent (Fig. 2d). As in tumours, *PTPN1*-KD BC cells underwent non-apoptotic death after exposure to 0.1% O_2 (Supplementary Fig. 4a, b).

Surprisingly, the increased death of *PTPN1*-deficient BC cells in low oxygen was not accompanied by defective activation of known hypoxia response pathways, including HIF1α, UPR or mTOR, as assessed by HIF1α stabilization and activity, and phosphorylation of eIF2α or S6, respectively (Supplementary Fig. 4c-g). Instead, HIF1α stabilization and eIF2α phosphorylation actually occurred earlier in some 1B-KD BC cells, suggesting that they might be experiencing more severe hypoxia than parental cells.

PTP1B regulates non-mitochondrial oxygen consumption, via multiple αKG-dependent dioxygenase(s)

We therefore sought other explanations for the hypoxia hypersensitivity of PTP1B-deficient BC cells. First, we asked if PTP1B deficiency affected oxygen consumption. To assess ATP-coupled respiration, maximal respiration and non-mitochondrial oxygen consumption[25], we measured the oxygen consumption rate (OCR) basally and in the presence of oligomycin (a mitochondrial (mt) ATPase inhibitor), FCCP (an uncoupling agent) or rotenone (mt complex I inhibitor) plus antimycin A (mt complex III inhibitor). Consistent with the observed HIF1α activation (see above), mitochondrial OCR was reduced in hypoxia-exposed parental and PTP1B-deficient cells, compared with their normoxic counterparts. In hypoxia-exposed conditions, however, the OCR was higher in *HER2+* (BT474) 1B-KD cells than in parental cells. This difference was also evident in normoxic conditions in the presence of oligomycin or when rotenone and antimycin A were added to block the electron transport chain (Fig. 3a). These results indicated that *non-mitochondrial* oxygen consumption (NMOC) was increased in BT474 1B-KD cells. Consistent with this notion, there was no increase in mitochondrial mass or activity in such cells (Supplementary Fig. 5a-c). The effects of PTP1B deficiency on cell survival were restricted to severe hypoxia (0.1%-0.5% O_2); survival of parental and 1B-KD cells was similar at higher oxygen concentrations (Fig. 3b). Moreover, 1B-KD and parental cells died at similar rates under anoxia. These findings suggest that in severe hypoxia, PTP1B-deficient *HER2+* BC cells fail to inhibit NMOC and thus deplete remaining oxygen reservoirs faster than parental cells.

In parallel, we analyzed metabolites in two *HER2+* BC (BT474 and SKBR3) cell lines using liquid chromatography-tandem mass spectrometry (LC-MS/MS). Principal component analysis revealed global alteration of the metabolome in the PTP1B-deficient cells, which was restored by mPTP1B expression (Supplementary Fig. 6a-e and Supplementary Table 1). Control and PTP1B-deficient BT474 and SKBR3 cells showed multiple PTP1B-dependent alterations in metabolite levels, but the only shared difference was an ˜2-fold lower level of α-ketoglutarate (α-KG) in PTP1B-deficient cells (Fig. 4a, b). This decrease could not be explained by consistent differences in the levels of glutamine metabolism enzymes or by altered isocitrate dehydrogenase (IDH) activity (Supplementary Fig. 5d and 6f).

Increased non-mitochondrial oxygen consumption, concomitant with decreased α-KG levels, could reflect increased activity of one or more α-KG-dependent dioxygenases (α-KGDDs)[6–9]. Consistent with this notion, there was an increase in the number and intensity of bands detected with anti-hydroxyproline antibodies in 1B-KD *HER2+* BC cells, which was reversed upon treatment with the generic α-KGDD inhibitor IOXI (Fig. 4c-h). Several α-KGDDs catalyse prolyl hydroxylation, so these differences could reflect increased activity of multiple (if not all) family members, not just those HIF1α hydroxylases. Carnitine biosynthesis requires another α-KGDD, γ-butyrobetaine dioxygenase (BBOX). Remarkably, carnitine levels were increased in PTP1B-deficient *HER2+* BC cells in normoxia or hypoxia (Fig. 4i), consistent with increased BBOX activity. DNA from PTP1B-deficient *HER2+* BC cells in normoxia or hypoxia also showed globally decreased reactivity to an antibody against 5-methyl cytosine, whereas reactivity was restored upon IOXI treatment (Fig. 4j, k). This finding could reflect increased activity of TET family DNA

demethylases, which also are α-KGDDs. Together, these results suggest that multiple α-KGDD-dependent pathways are activated in PTP1B-deficient *HER2+* BC cells.

Most importantly, pre-treatment with the generic α-KGDD inhibitors IOXI or DMOG26–28 protected 1B-KD *HER2+* BC cells from hypoxia-induced death in a dose-dependent manner (Fig. 5a, b), and normalized the increased NMOC in PTP1B-deficient cells (Fig. 3e). As expected, IOXI addition decreased maximal OCR, consistent with HIF1α stabilization as a consequence of HIF prolyl hydroxylase inhibition. Together, these findings suggest that PTP1B controls the activity of one or more α-KGDDs to regulate NMOC and, potentially, α-KG levels.

RNF213 is a putative PTP1B substrate

Our results show that PTP1B catalytic activity is required to prevent hypoxia hypersensitivity. To search for PTP1B substrates that might mediate hypoxia hypersensitivity in the absence of PTP1B, we stably expressed Flag-m*Ptpn1* WT or an m*Ptpn1* "substrate-trapping" mutant (CS/DA) in BT474 1B-KD cells. mPTP1B CS/DA is a double mutant of the catalytic cysteinyl residue (C215S) and the aspartyl residue (D181A) that acts as a general acid to effect PTP catalysis; such mutants can bind, but not promote hydrolysis of, substrates29. As reported previously30, Flag-mPTP1B CS/DA "trapped" the EGFR from lysates of EGF-stimulated cells (Supplementary Fig. 7a). Unbiased MS identification of potential mPTP1B substrates from normoxic or hypoxic cells did not identify known α-KGDDs or α-KGDD regulators. Instead, two proteins, ARHGAP12 and RNF213, were enriched substantially in Flag-mPTP1B CS/DA co-immunoprecipitations (Supplementary Fig. 7b). ARHGAP12 is a RHO-GTPase-activating protein (a.k.a., RHOGAP12) thought to be involved in cell motility31, and was suggested to be a PTP1B substrate in an earlier proteomic study32. We confirmed the preferential interaction of ARHGAP12 with substrate-trapping mutants; however, *ARHGAP12* depletion (with siRNA) had no effect on the hypoxia sensitivity of parental or 1B-KD *HER2+* BC cells (Supplementary Fig. 7c, d).

RNF213 is a 591kDa protein containing a RING E3-ligase and an AAA+ ATPase domain33, but had not previously been implicated in PTP1B action. We validated the interaction of RNF213 with PTP1B-CS/DA and with another trapping mutant, PTP1B-D/A, by immunoblotting (Fig. 6a). PTP1B/RNF213 interaction appears to require the PTP1B catalytic center, because the competitive inhibitor sodium vanadate (Na_3VO_4) preferentially interfered with RNF213 binding to Flag-mPTP1B DA, which retains its active site cysteine, compared with Flag-mPTP1B CS/DA (Fig. 6b). Consistent with these observations, RNF213 is tyrosine-phosphorylated, although there was no obvious difference in overall phosphotyrosine (pY) levels on RNF213 in parental versus 1B-KD *HER2+* BC cells (Fig. 6c). The latter result suggests that PTP1B targets specific sites on RNF213. Most importantly, *RNF213*-knockdown rescued multiple 1B-KD *HER2+* BC cells from hypoxia-induced cell death (Fig. 6d). Furthermore, whereas *RNF213*-KD alone had minimal effects on OCR, it corrected the increased NMOC in BT474 1B-KD cells to levels comparable to parental cells (Fig. 6e), normalized the increase in IOXI-dependent, hydroxyproline antibody-reactive bands (Fig. 6f) and restored DNA methylation to parental levels (Fig. 4k).

In addition, *RNF213*-KD decreased HIF1α hydroxylation in 1B-KD, but not parental, *HER2+* BC cells, providing evidence that PTP1B/RNF213 can regulate specific hydroxylation events (Supplementary Fig. 7e, f). Finally, *RNF213*-KD partially (but significantly) restored the growth of 1B-KD HCC1954 tumours (Fig. 6g-i and Supplementary Fig. 7g-i), while normalizing their increased staining with EF5.

PTP1B regulates RNF213 E3 activity and globally affects ubiquitylation in HER2+ BC cells

The above findings indicated that PTP1B negatively regulates RNF213. To examine the biochemical effects of PTP1B on RNF213 and to identify potential RNF213 substrates, we expressed HA-tagged ubiquitin (HA-Ub) in Control and 1B-KD *HER2+* cells. Remarkably, PTP1B deficiency or inhibition substantially increased overall ubiquitylation (by immunoblotting), and much of this increase was suppressed by *RNF213*-KD (Fig. 7a-d and Supplementary Fig. 7j, k). We also generated *RNF213* knockout (*RNF213*-KO) BT474 cells by using the CRISPR/*Cas9* system. Consistent with the effects seen in *RNF213*-KD cells, PTP1B inhibitor treatment resulted in increased ubiquitylation in BT474 cells, but not in the *RNF213*-KO cells (Fig. 7e). *RNF213*-KD or –KO alone also decreased overall ubiquitylation in parental BT474 cells. As noted above, IOXI protected PTP1B-deficient *HER2+* BC cells from hypoxia-induced death, but it did not normalize the increased level of ubiquitylated proteins in these cells (Supplementary Fig. 7l). Hence, αKGDD regulation is downstream of RNF213.

We used two distinct, but complementary, methods, HA-Ub IP-MS and DiGly IP-MS, to identify and quantify changes in the ubiquitylome (Supplementary Fig. 7m and Supplementary Table 2, 3)34. Consistent with the results of our immunoblotting experiments, nearly 40% of the ubiquitylome was increased in 1B-KD BT474 cells, and most (>60%) of this increase was suppressed by *RNF213*-KD (Fig. 7f). Pathway analysis of PTP1B/RNF213-dependent ubiquitylated proteins revealed marked enrichment for proteins involved in ubiquitin-mediated proteolysis (E1s, E2s, E3s and deubiquitylases; Supplementary Table 4).

These results suggested that PTP1B negatively regulates RNF213 E3-ligase activity. Indeed, RNF213 auto-ubiquitylation activity was enhanced in 1B-KD BT474 cells, compared with their parental counterparts (Fig. 7g). Regulation of multiple proteins involved in ubiquitin-mediated proteolysis by RNF213 could explain the large changes in ubiquitylation in PTP1B-deficient *HER2+* BC cells.

Discussion

We have discovered that PTP1B is required for the survival of *HER2+* BC cells in severe hypoxia. Genetic and biochemical evidence suggest that RNF213 is a PTP1B substrate, which in turn controls the activity of one or more IOXI/DMOG-sensitive α-KGDDs (Fig. 7h). We propose that, in normoxic conditions, the excess NMOC caused by these enzymes in PTP1B-deficient cells can be tolerated. By contrast, in the hypoxic tumour microenvironment, excessive NMOC (caused by increased α-KGDD activity) results in oxygen depletion and necrotic cell death (Fig. 7h). Therefore, in parallel to the well-described regulation of mitochondrial oxygen consumption by HIF, control of NMOC by

this PTP1B/RNF213/α-KGDD pathway, appears to be essential for hypoxic survival of tumour cells. Our results also identify RNF213 as a major regulator of the ubiquitylome, at least in *HER2*^{+} BC cells.

Ptpn1 deficiency impairs the ability of oncogenic alleles of *Neu* (rat HER2) to cause BC in mice19,20. But whereas Julien *et al.* reported decreased ERK and AKT activation in tumours that eventually arose in the PTP1B-deficient animals20, we saw no consistent effect on ERK or AKT in the rare tumours that arose in compound mutant mice19. We did observe a consistent decrease in ERK activity in PTP1B-deficient hyperplastic lesions, but these changes were small and of uncertain biological consequence. Similarly, we observed no effect of PTP1B deficiency or inhibition on cell proliferation, viability or HER2 signalling events in human BC lines *in vitro* or in the tumours. Recently, Krishnan *et al.* reported that MSI-1436, an allosteric inhibitor of PTP1B, impaired HER2 cell proliferation *in vitro*22. Notably, those experiments used surrogate assays for proliferation rather than the direct cell counts used here.

Several lines of evidence indicate that RNF213 is a substrate of PTP1B, and that PTP1B negatively regulates RNF213. First, RNF213 preferentially binds to two substrate-trapping mutants of PTP1B. Interaction with the substrate-trapping mutant containing an intact catalytic cysteine (DA) is preferentially disrupted by the competitive inhibitor sodium orthovanadate, compared with the trapping mutant (CS/DA) without a catalytic cysteine. These results suggest direct interaction between RNF213 and the PTP1B catalytic center. Furthermore, RNF213 from PTP1B-deficient cells shows increased *in vitro* auto-ubiquitylation activity. Nevertheless, tyrosine phosphorylation of RNF213 is not increased in PTP1B-deficient/inhibited cells. We suspect that only a specific tyrosine(s) is regulated by PTP1B; nevertheless, RNF213 should be viewed as a putative substrate until such residues are identified. Regardless, our *RNF213*-KD and –KO experiments show clearly that RNF213 is the essential downstream mediator of the effects of PTP1B on hypoxia sensitivity. Conceivably, the vascular occlusions, increased VEGF production, and abnormal blood vessel generation33,35,36 in Moyamoya disease also reflect a de-regulated hypoxia response.

Our results also link RNF213 to the control of α-KGDDs. Although the precise mechanism is unclear, we suspect that one or more RNF213 substrates globally regulate α-KGDDs by altering the levels of co-substrates/metabolites, such as ascorbate and/or iron. It also is tempting to speculate that sub-clinical deficiency of these substances could represent a contributing environmental factor(s) in Moyamoya disease pathogenesis.

Although we focused on the role of PTP1B in *HER2*^{+} BC, *PTPN1* is amplified in other malignancies, including colorectal (10.1%), and ovarian (8%) cancers37. Future work will focus on whether PTP1B has a broader role in controlling hypoxic survival in tumours and on defining the function, substrates and regulators of RNF213. Such studies could suggest new therapeutic approaches for *HER2*^{+} BC and other malignancies. Although small molecule inhibitors of PTP1B have been sought primarily for the treatment of diabetes and obesity, our results suggest that PTP1B inhibition, perhaps in combination with agents that preferentially kill normoxic cells (e.g., radiation) or drive tumours towards a hypoxic state

(e.g., anti-angiogenics), could be beneficial in cancer therapy. Finally, it will be important to clarify the potential role of PTP1B, αKGDDs and NMOC in Moyamoya disease pathogenesis.

Methods

Reagents

PTP Inhibitor XXII (CAS 765317-72-4)[38] was purchased from EMD Millipore. IOXI (CAS 5852-78-8) was purchased from Cayman Chemicals. Oligomycin A, FCCP (trifluorocarbonylcyanide phenylhydrazone), rotenone, and DMOG (Dimethyloxaloglycine) were purchased from Tocris Bioscience. Antimycin A was purchased from Enzo Life Sciences.

Rabbit polyclonal anti-RNF213 antibodies were generated and used as described[39]. Other antibodies were purchased and used for immunoprecipitations and/or immunoblotting at manufacturer-recommended concentrations (Supplementary Table 5).

Cell Culture, Infections and Transfections

Breast cancer lines were purchased from the American Type Culture Collection or Deutsche Sammlung von Mikroorganismen und Zellkulturen. No lines used in this study are found in the ICLAC or NCBI Biosample databases of commonly misidentified cell lines. All cell lines were authenticated by STR profiling (GenePrint® 10 System – 10 marks, Centre for Applied Genomics, Hospital for Sick Children, Toronto), and tested for mycoplasma (MycoAlert™ Lonza). BT474, SKBR3, MDA-MB-361 and JIMT1 cells were maintained in DMEM+10% FBS. HCC1954 cells were cultured in RMPI+10% FBS. Where indicated, cells were stably infected with VSVG-pseudotyped retroviruses carrying pSuper-puro shControl or sh*PTPN1* or VSVG-pseudotyped lentivirus harboring pLKO (901)-IPTG-inducible-puro sh*PTPN1*. Reconstitution of PTP1B was achieved by infecting cells with the VSVG-pseudotyped retrovirus pFB-neo m*Ptp1b*–wild-type, the catalytically impaired m*Ptp1b* mutant (R221M), Flag-*mPtp1b*–wild-type or a Flag-substrate-trapping mutant (D181A or D181A/C215S). To obtain stable transductants, infected cells were treated with 1.5μg/ml (BT474/SKBR3), 3μg/ml (MDA-MB-361), 4μg/ml (HCC1954), or 7μg/ml (JIMT1) puromycin (Bioshop) for 3 days or with 700μg/ml G418 (Bioshop) for 7 days. Smartpools™ or individual siRNAs for *RNF213, ARHGAP12* and *IDH1* (Thermo Scientific) were introduced into cells using Lipofectamine RNAiMAX (Invitrogen), per the manufacturer's instructions. All RNAi and shRNA sequences are shown in Supplementary Table 6.

For soft-agar assays, 5,000 cells were mixed into 0.3% agar (top layer), and seeded onto 10 cm plates containing a 0.6% agar (bottom) layer. Media were changed every 4 days for 4 weeks. Images were obtained at 4x magnification using a Leica DFC420 digital camera and Leica FireCam software. Colonies were counted in 10 fields using a $0.25cm^2$ grid.

For Matrigel assays, 48-well plates were coated with 3-D Culture Matrix™-Reduced Growth Factor Basement Membrane Extract (Cultrex), and incubated at 37ºC for 30 mins.

Each well was seeded with 5,000 cells in 500 µl of growth media. Media were changed every 4 days for 3 weeks, and images were obtained as above.

Xenografts, Mouse Models and Histology

Breast cancer cells (1×10^6) were suspended in 40 µl of 50% growth factor-reduced Matrigel (BD Science), and injected sub-cutaneously into the right flanks of 6-8 week-old female Balb/c athymic nude mice implanted with (BT474 and MDA-MB-361) or without (JIMT1 and HCC1954) a 60-day release pellet containing 0.72 mg 17β-estradiol (Innovative Research of America). Experiments were not randomized, nor were the investigators blinded to allocation during experiments and outcome assessment. Tumours were measured weekly with calipers, and tumour volume was calculated as length x width^{2}x 0.52 (Ref. 40). For tumour maintenance experiments, IPTG (1 mM) was added to the drinking water to induce expression of *PTPN1* shRNA. No statistical method was used to pre-determine sample size, but based on the results of a pilot experiment consisting of 9 mice each for parental and 1B-KD BT474 tumours, power analysis indicated that 8 mice/group were sufficient to detect an approximately three-fold difference in mean tumour size. *Ptpn1$^{-/-}$* and *MMTV-Neu^{NT}* mice (mixed background, 129/B6/FVB) were described previously41. Females containing one copy of *MMTV-Neu^{NT}* from *Ptpn1$^{+/-}$* x *MMTV-Neu^{NT}; Ptpn1$^{+/-}$* crosses were kept as virgins for the entire study period. Mice that died for unknown reasons were excluded from analysis. All animal studies were approved by the University Health Network Animal Care Committee (Protocol #1239).

Before euthanizing, mice were injected with 1.5mg BrdU and 2µmoles EF5 for 24 hrs or 4 hrs, respectively. Tumours and mammary glands were fixed in formalin and embedded in paraffin. Sectioning and H&E staining were performed by the University Health Network Pathology Research Program (UHN PRP, Toronto, ON, Canada). Immunohistochemical analyses were performed by the UHN PRP or the Princess Margaret Cancer Centre Applied Molecular Profiling Laboratory (AMPL). See http://www.uhnres.utoronto.ca/programs/ampl/index.html for details on staining conditions. Slides were scanned at the Princess Margaret Cancer Center Advanced Optical Microscopy Facility, and analyzed with Aperio ImageScope software (Leica Biosystems). In each sample, the percentage of EF5 staining was normalized to tumour size.

In vitro hypoxia assays

Cells were seeded at 2×10^6 cells/60 mm plate (4×10^6/plate for MDA-MB-361), and allowed to adhere overnight. The next day (Day 0), cells were counted, and the media (3 ml) was exchanged, before replicates were placed into a standard incubator (normoxia), tri-gas incubator (5% O_2, Sanyo MCO-18M), hypoxia chamber (0.1%-1.0% O_2, Whitley H35 Hypoxystation) or anoxic chamber (0% O_2, Whiteley H85 Hypoxystation). PTP1B inhibitor and/or the oxygenase inhibitors IOXI or DMOG were added after the media was changed on Day 0, but before placing cells in the normoxia or hypoxia chamber. Cells remaining on the plate were counted at the indicated times. Experiments were scaled up or down onto different sized plates based on surface area. For colony formation assays, cells were exposed to normoxia or 0.2% O_2 hypoxia for 24 hrs, and then reseeded onto 10cm plates at the

indicated densities in triplicate. Media were changed every three days for 3-4 weeks. Colonies were stained using methylene blue and counted.

Generation of RNF213 knockout BT474 cells

An *RNF213*-knockout BT474 cell line was generated by CRISPR/*Cas9*-mediated genome engineering42. Briefly, a target sequence in the third exon of *RNF213* (ACAATGGCGTCGGCCTCGGA) was designed by consulting the website http:// crispr.mit.edu, and cloned into the *BbsI* site of *pSpCas9 (BB)-2A-GFP (PX458)* (Addgene). BT474 cells were transfected with the PX458-sgRNF213 vector using FuGENE® 6 Transfection Reagent (Promega). Forty-eight hours post-transfection, GFP-positive cells were sorted, cultured at limiting dilution and single clones were isolated. Homozygous *RNF213* mutation was identified by DNA sequencing and confirmed by immunoblotting.

Flow cytometry

Cell death was analyzed by Sytox Blue® and Annexin V staining. Culture supernatants and trypsinized cells were collected, combined and recovered by centrifugation at 365 x g in a table top centrifuge (Beckman Coulter). Cells were washed with Hanks' Balanced Salt Solution (HBSS, Wisent), resuspended in 1X Annexin V binding buffer (BD Science) and stained with Annexin V-PI (BD Pharmingen) and Sytox blue (Invitrogen), as recommended by the manufacturers. Total and active mitochondria were stained with Mitotracker™ dyes (Invitrogen). Cells were stained with 200 µM of Mitotracker Green and CMXROS (both from Invitrogen) for 30 min. All samples were analyzed using a Becton Dickinson (BD) LSRII (BD Biosciences) and FlowJo software.

Quantitative Real-Time PCR

Cellular RNA was extracted by using the miRNeasy kit (Qiagen), and then reverse transcribed using the RT2 first stand kit (Qiagen). The resultant cDNA (20ng) was mixed with SYBR Green Supermix (Qiagen and Life technologies), along with primers specific to HIF1α target genes, as described previously43, or analyzed by using the RT2 profiler™ PCR array – human hypoxia signaling pathway (See Supplementary Table 7). Reactions were performed on the CFX96 real-time PCR machine (Bio-Rad). CT was calculated using *RPL13A* as a loading control. Fold-change was calculated relative to parental *HER2+* breast cancer cells in normoxia.

Oxygen consumption measurements

Oxygen consumption rate (OCR) was measured with an XF96 analyzer (Seahorse Bioscience). Briefly, cells (25,000/well) were seeded in DMEM (no buffer) + 2%FBS in 96 well plates. The plates were centrifuged at $21 \times g$ in a table top centrifuge (Beckman Coulter) with no deceleration for 5 min, before placement into the analyzer. Injection ports were loaded to achieve the following final working concentrations: oligomycin A (1.5 µM), FCCP (1 µM), rotenone (1 µM) and antimycin A (1 µM). Before OCR measurements, cells were exposed to normoxia or 0.1% O_2 hypoxia for 24 hrs, treated with IOXI overnight (16 hrs), or transfected with siRNAs for 72 hrs, as indicated.

Metabolomics

Metabolites were prepared as described44. Briefly, cells were flash frozen in liquid N_2, and extracted with 40% acetonitrile:40% methanol:20% H_2O. Extracts were placed into 1.5 ml Eppendorf tubes (Corning), vortexed at 4°C for 1 hr and centrifuged at 4°C for 10 mins at ~18,000 x g in an Eppendorf microfuge. Supernatants were evaporated in a Speedvac (Acid-Resistant CentriVap Vacuum Concentrators, Labconco), and samples were resolved by LC-MS/MS. Analysis was performed in positive and negative modes at the optimum polarity in MRM mode on an electrospray ionization (ESI) triple-quadrupole mass spectrometer (ABSciex4000Qtrap, Toronto, ON, Canada), as described44–46. Some metabolites appear in duplicate due to using different ions to confirm the metabolites. Principal component analysis and heat maps were generated by using Mass Profiler Professional (Agilent).

DNA methylation dot blots

Genomic DNA and methylated DNA standards (Cat. #55008; Active Motif) were heat-denatured in 0.4 M NaOH (Sigma) & 10 mM EDTA (Sigma) at 100 °C for 10 min and chilled on ice for 5 min. Samples were two-fold serially diluted and applied to a positively charged nylon membrane (Biodyne B; Pall Life Sciences) using the Bio-dot microfiltration apparatus (Biorad). Membranes were UV-crosslinked at 12,0000 μJ/cm2 (CL1000; UVP), and blocked in TBS, 0.1% Tween-20 (TBST), 5% milk for 1 hr. Primary antibodies against 5-mC (1:1000; cat. 39649; Active Motif) were incubated with the membrane in TBST overnight. Dot blots were washed 3X in TBST, incubated in HRP-conjugated IgG secondary antibodies (GE healthcare) for 1hr, and detected by standard ECL methods (Supersignal West Pico; Thermo Fisher Scientific).

Immunoblotting and Immunoprecipitation

For immunoblotting, whole cell lysates were generated in modified radioimmunoprecipitation (RIPA) buffer (50mM Tris-HCl pH 8.0, 150mM NaCl, 2mM EDTA, 1% NP-40, and 0.1% SDS, without sodium deoxycholate). TNE lysis buffer (50mM Tris-HCl pH 8.0, 150mM NaCl, 2mM EDTA, and 1% NP-40) was used for immunoprecipitations. Lysis buffers were supplemented with protease (40μg/ml PMSF, 2μg/ml antipain, 2μg/ml pepstatin A, 20μg/ml leupeptin, and 20μg/ml aprotinin) and phosphatase (10mM NaF, 1mM Na_3VO_4, 10mM β-glycerophosphate, and 10mM sodium pyrophosphate) inhibitors. Lysates were incubated, as indicated, with anti-RNF213 antibodies and G-Sepharose 4 Fast Flow (GE Healthcare) or anti-Flag M2 agarose (Sigma-Aldrich) for 3 hrs at 4°C on a rotating platform. Beads were washed 4X in their respective lysis buffer, and then analyzed by immunoblotting, essentially as described47. To detect RNF213, lysates and immunoprecipitates were resolved by modified SDS-PAGE, using 3-8% Tris-acetate gels and Tris-acetate running buffer (Invitrogen). Tris-acetate gels were transferred in 1X transfer buffer, 10% methanol and 0.1% SDS. All other proteins were resolved by standard SDS-PAGE, and transferred using 1X transfer buffer and 15% methanol47. Membranes were incubated with their respective primary antibodies, and visualized with IRDye infrared secondary antibodies, using an Odyssey Infrared imaging system (Li-Cor Biosciences).

Isocitrate Dehydrogenase (IDH) Activity measurements

IDH activity was measured as described[48,49]. Briefly, cells were lysed in PBS + 0.1% Triton-X-100, supplemented with protease inhibitors as above. Aliquots of each lysate (4 μg protein) were added to assay buffer [25mM Tris-HCl pH 7.5, 0.5mM EDTA, 1.5mM $MnCl_2$, 1.0mM isocitrate], and OD_{340} was measured with a plate reader every 30 seconds. Backgrounds (wells without lysate) were subtracted to yield OD_{340} values.

Protein Mass Spectrometry

Cells were lysed in MS buffer (50mM Hepes pH 7.0, 100mM KCl, 0.5% NP-40, 2mM EDTA, 10% glycerol), supplemented with protease and phosphatase inhibitors, as above. Lysates were immunoprecipitated with 80μl of a 50% slurry of M2 Flag-agarose beads (Sigma-Aldrich) for 3 hrs at 4°C on a rotating platform. Beads were washed 3X in MS buffer, and 4X in rinse solution (50 mM NH_4HCO_3 and 75mM KCl), and then eluted with three aliquots (250μl each) of 0.5M NH_4OH. Pooled eluates were lyophilized, trypsinized, passed through C18 ZipTip® Pipette Tips (Millipore), and subjected to LC-MS/MS on a Q-Exactive MS (Thermo Scientific). Data were analyzed with Proteome Discoverer (Thermo scientific), followed by Scaffold (Proteome Software), using the Uniprot database.

Ubiquitylome Analysis

Cells were transfected with empty pBabe-puro vector or pBabe-puro expressing HA-tagged ubiquitin (HA-Ub) using Fugene 6 (Promega), per the manufacturer's instructions. Transfected cells were exposed to normoxia or 0.1% O_2 for 24 hrs, and treated with and without 10μM MG132 and 50μM Chloroquine to inhibit the proteasome and lysosome, respectively. Cells were lysed in RIPA buffer (+10mM IAM and NEM) and lysates were analyzed by immunoblotting as described above.

For HA-Ub IP-MS, cells were lysed in RIPA buffer, and lysates were immunoprecipitated with 100μl of a 50% slurry of HA-agarose beads (Sigma-Aldrich) overnight at 4°C on a rotating platform. Beads were washed 3X in RIPA buffer, 4X in rinse solution and then eluted with three aliquots (250ul each) of 0.1% trifluoroacetic acid (TFA). Samples were prepared and cleaned as described in *Protein Mass Spectrometry*. Lyophilized peptide pellets were re-suspended in 10 μL of 0.1% formic acid. LC-MS/MS was performed as described[50], except the entire 10 μL of sample was injected for each analysis.

MaxQuant version 1.5.1.0 was used to search raw data from the mass spectrometer against using the UniProt complete human proteome sequence database (version: 2012-07-19, number of sequences: 20,232)[51]. Carbamidomethylation of cysteines was defined as a fixed modification, and oxidation of methionine and acetylation of protein N-termini as variable modifications. False discovery of peptides was controlled using a target-decoy approach, where peptides under the threshold of 1% false discovery rate were carried on for analysis. Subsequently, protein groups identified with at least two or more peptides were carried forward in analysis. All post-search and statistical analysis of proteomics data was performed using R. LFQ intensities assigned to protein groups were used as a proxy for protein intensities; however, missing LFQ intensities were substituted by adjusted iBAQ

intensities. Remaining missing data were imputed with a constant value. Further details are available from A.S. or T.K.

For diGly enrichment, proteins were extracted from cells by adding lysis buffer (8M urea, 150mM NaCl, 50mM HEPES [pH 7.5], 1mM EDTA, protease inhibitor [Roche]), and passing the cells 20 times through a 21G needle. Proteins were reduced with 10mM TCEP, alkylated with 15mM NEM, and capped with 10mM DTT. Prior to digestion, proteins were precipitated with chloroform/methanol, and the pellet was re-suspended in 8M urea, 50mM HEPES using a syringe, as described above. Proteins were diluted in 50mM HEPES to 4M urea, and digested with LysC (1:100 enzyme:substrate ratio) for 6 hours at 30°C. This solution was diluted to 1M urea with 50mM HEPES before the addition LysC and Trypsin (1:100 enzyme:substrate) and incubation at 37°C overnight. Before enrichment, peptides were acidified before desalting by passage over C-18 solid phase extraction (SPE) columns (Waters, Milford, MA).

The anti-diGly antibody was cross-linked to protein A agarose beads, as described. Lyophilized peptides from 11 mg of protein were dissolved in 1.5 mL of IAP buffer (50mM MOPS [pH 7.5], 10mM Na_2HPO_4, 50mM NaCl), and centrifuged at maximal speed for 5 min to remove insoluble material. Supernatants were removed, and incubated for 2 hr at 4°C with anti-diGly antibody (Cell Signaling Technologies, Danvers, MA; 32 μg/IP), cross-linked to protein A agarose as described[52]. Following binding, supernatants containing unbound peptides were retained, and the beads were washed 2X with IAP and 3X with PBS before elution of enriched peptides with 0.15% TFA. A second enrichment was performed using the unbound peptides from the first enrichment. Eluted peptides were desalted by using a C-18 stage tip.

Isobaric labeling of peptide eluates was performed using 10-plex tandem mass tag (TMT) reagents (Thermo Fisher Scientific, Rockford, IL)[53]. Before use, TMT reagents (0.8mg) were dissolved in 40 μL of anhydrous acetonitrile (ACN). Dry, enriched peptides were dissolved in 18μL of 200mM HEPES (pH 8.0) and 4μL anhydrous ACN. Labeling was performed by the addition of 3μL TMT, followed by incubation at room temperature for 1 hour. Reactions were quenched with 2μL of 5% hydroxylamine [3% v/v hydroxylamine]. Samples were mixed and desalted by Stage Tip before analysis by mass spectrometry.

Spectra were acquired on an Orbitrap Fusion mass spectrometer, coupled to an Easy-nLC 1000 (Thermo Fisher Scientific, San Jose, CA)[54]. Peptides were separated over an analytical column (100 μm ID) packed with 0.5cm of Magic C-18 (5μm, 100A, Michrom Bioresources) and 35cm of Sepax Technologies GP-C18 resin (1.8μm, 120A, Newark, DE), using a linear gradient from 8 to 26% ACN with 0.125% formic acid over 180 min at a flow rate of 450 nL/min. High resolution (120,000 resolving power, AGC = 200,000) survey scans (MS1) were used to guide data-dependent sampling and subsequent CAD fragmentation (NCE = 35) of the top ten most-intense peptides. MS2 fragment ions were analyzed in the ion trap (MS2 AGC = 5,000, MS3 AGC = 50,000), and the top 10 fragment ions were isolated by synchronous precursor selection, fragmented by HCD (NCE = 55) to produce TMT 10-plex reporter ions, and analyzed in the Orbitrap at a resolution of 60,000[55,56]. Precursors with unassigned or +1 charge states were excluded, and previously

interrogated precursors were excluded using a dynamic window (60s, +/- 10 ppm) around the assigned monoisotopic peak.

A compilation of in-house software was used to convert mass spectrometric data to mzXML format, as well as to correct monoisotopic m/z measurements and erroneous peptide charge state assignments. MS/MS spectra were mapped to peptide sequences by using SEQUEST[57] to search an *in silico* tryptic digest (2 missed cleavages) of a Uniprot protein database containing target and decoy human proteins, as well as known contaminants. SEQUEST searches allowed a 50 ppm precursor ion tolerance and a 0.9Da fragment ion tolerance. TMT labels on peptide N termini/lysine residues (+229.16293Da) and n-ethylmaleimide on cysteine residues (+125.12528Da) were set as static modifications, whereas methionine oxidation (+15.99492Da) and the di-glycine ubiquitin remnant modification of lysine residues (+114.04293Da) were set as dynamic modifications. Peptide spectral matches were filtered to 1% FDR by applying the target-decoy strategy, as described[58]. Subsequently, proteins were grouped and filtered to 1% FDR[56]. Following protein grouping, a modified version of Ascore was used to confidently (P ≤ 0.05) localize ubiquitinylation sites (Ascore > 13)[59].

Analysis of HA-Ub IP-MS was performed on two independent biological replicates. Increases and decreases from LFQ and pINT (LFQ + iBAQ) were combined and scored if they appeared in either biological replicate. Proteins from the diGly list were scored if at least one peptide was increased in *PTPN1*-KD cells alone, decreased in *RNF213*-KD cells alone or increased in *PTPN1-KD* cells and decreased in *RNF213-KD* cells, as indicated in the figure and table legends.

Autoubiquitylation Assays

BT474 parental and 1B-KD cells were transfected with 3xFlag-RNF213 WT with Fugene 6 (Promega), following manufacturer's instructions. Transfected cells were placed in normoxia for 24 hrs, lysed with TNE lysis buffer, followed by anti-Flag M2 agarose co-immunoprecipitation, as described above. Auto-ubiquitylation assays were performed in a buffer (30μL, 1.5X beads volume) containing 50mM Tris-Cl pH8.0, E1/UBE1 (250nM, Boston Biochem), E2/UBE2D2 (10μM, Boston Biochem), ubiquitin (20μM, Boston Biochem), ATP (2mM) and $MgCl_2$ (10mM). After incubation at 37°C for 60 min, reactions were terminated by the addition of SDS-PAGE sample buffer, and resolved using 3-8% Tris-aceetate gradient SDS-PAGE gels, as described above. Ubiquitylated RNF213 species were visualized by immunoblotting, using anti-RNF213 rabbit polyclonal antibodies, as indicated.

Bioinformatic Analyses

Proteins showing ≥ 1.5 fold increased ubiquitylation in *PTPN1*-KD cells, ≤ 0.67 fold decreased ubiquitylation upon *RNF213*-KD or that were affected both by *PTPN1*-KD and *RNF213*-KD were compared to find common sets of overlapping proteins[60] by using the BinGO (v3.0.3)[61] plugin. The May 2015 GO definition file was used as the baseline, and each high-level GO category (Biological Process, Cellular Component, Molecular Function) was tested (hypergeometric test, Benjamini-Hochberg FDR q<0.05) independently. To assess

KEGG pathways and INTERPRO domains enriched in each of the lists, the online tool DAVID62 was used (default settings, background human genome).

Statistics and Reproducibility

Sample sizes and statistical tests for each experiment are denoted in the figure legends. Raw data from independent replicate experiments are found in Supplementary Table 8. Each dot-blot and immunoblot was performed at least twice if more than one cell line was studied or at least three times if only a single line was used. All xenografts represent one independent experiment with the indicated biological replicates and each immunoblot contained multiple tumor lysates (biological replicates) from each group. All metabolomics data represent $n=5$ technical replicates for each group from a single independent experiment. All immunohistochemical images show samples from a single mouse of each group, and quantification was performed on all biological replicates in the experiment, with the number of data points indicating the number of independent biological replicates. Non-normally (skewed) distributed data (Fig. 2d) was normalized by log2-transformation. The multi-level t-test was implemented using the R package "*nlme*" (https://cran.r-project.org/web/packages/nlme). The between-group variances were similar, and the data were normally distributed. All analyses and graphs were generated with GraphPad Prism 5. A *p*-value of <0.05 was considered significant, precise *p*-values can be found in the figures.

Data Availability

The raw LC-MS/MS metabolomics data have been deposited at http://www.peptideatlas.org/PASS/PASS00871. Source data for Fig. 2a-d, 3a-b, 5a-b, 6d-e and Supplementary Fig. 1b-c, 4b, 4f, 5b-c, 6f, 7e-f have been provided in Supplementary Table 8 – Statistic Source Data. All other data supporting the findings of this study are available from the corresponding author upon reasonable request.

Supplementary Material

Refer to Web version on PubMed Central for supplementary material.

Acknowledgements

References

1. Bertout JA, Patel SA, Simon MC. The impact of O2 availability on human cancer. Nature reviews. Cancer. 2008; 8:967–975. DOI: 10.1038/nrc2540 [PubMed: 18987634]

2. Papandreou I, Cairns RA, Fontana L, Lim AL, Denko NC. HIF-1 mediates adaptation to hypoxia by actively downregulating mitochondrial oxygen consumption. Cell metabolism. 2006; 3:187–197. DOI: 10.1016/j.cmet.2006.01.012 [PubMed: 16517406]

3. Ma XM, Blenis J. Molecular mechanisms of mTOR-mediated translational control. Nature reviews. 2009; 10:307–318. DOI: 10.1038/nrm2672

4. Laplante M, Sabatini DM. mTOR signaling in growth control and disease. Cell. 2012; 149:274–293. DOI: 10.1016/j.cell.2012.03.017 [PubMed: 22500797]

5. Ron D, Walter P. Signal integration in the endoplasmic reticulum unfolded protein response. Nat Rev Mol Cell Biol. 2007; 8:519–529. [PubMed: 17565364]

6. Loenarz C, Schofield CJ. Expanding chemical biology of 2 oxoglutarate oxygenases. Nature chemical biology. 2008; 4:152–156. DOI: 10.1038/nchembio0308-152 [PubMed: 18277970]

7. Schofield CJ, Ratcliffe PJ. Oxygen sensing by HIF hydroxylases. Nature reviews. 2004; 5:343–354. DOI: 10.1038/nrm1366

8. Hewitson KS, Granatino N, Welford RW, McDonough MA, Schofield CJ. Oxidation by 2 oxoglutarate oxygenases: non-haem iron systems in catalysis and signalling. Philos Trans A Math Phys Eng Sci. 2005; 363:807–828. discussion 1035-1040. DOI: 10.1098/rsta.2004.1540 [PubMed: 15901537]

9. Schofield CJ, Zhang Z. Structural and mechanistic studies on 2-oxoglutarate-dependent oxygenases and related enzymes. Current opinion in structural biology. 1999; 9:722–731. [PubMed: 10607676]

10. Kuiper C, Vissers MC. Ascorbate as a co-factor for fe- and 2-oxoglutarate-dependent dioxygenases: physiological activity in tumor growth and progression. Front Oncol. 2014; 4:359.doi: 10.3389/fonc.2014.00359 [PubMed: 25540771]

11. Elchebly M, et al. Increased insulin sensitivity and obesity resistance in mice lacking the protein tyrosine phosphatase-1B gene. Science (New York, N.Y. 1999; 283:1544–1548.

12. Zabolotny JM, et al. PTP1B regulates leptin signal transduction in vivo. Developmental cell. 2002; 2:489–495. [PubMed: 11970898]

13. Klaman LD, et al. Increased energy expenditure, decreased adiposity, and tissue-specific insulin sensitivity in protein-tyrosine phosphatase 1B-deficient mice. Molecular and cellular biology. 2000; 20:5479–5489. [PubMed: 10891488]

14. Bettaieb A, et al. Protein tyrosine phosphatase 1B regulates pyruvate kinase M2 tyrosine phosphorylation. The Journal of biological chemistry. 2013; 288:17360–17371. DOI: 10.1074/jbc.M112.441469 [PubMed: 23640882]

15. Krishnan N, Fu C, Pappin DJ, Tonks NK. H2S-Induced sulfhydration of the phosphatase PTP1B and its role in the endoplasmic reticulum stress response. Science signaling. 2011; 4:ra86.doi: 10.1126/scisignal.2002329 [PubMed: 22169477]

16. Stuible M, Doody KM, Tremblay ML. PTP1B and TC-PTP: regulators of transformation and tumorigenesis. Cancer metastasis reviews. 2008; 27:215–230. DOI: 10.1007/s10555-008-9115-1 [PubMed: 18236007]

17. Comprehensive molecular portraits of human breast tumours. Nature. 2012; 490:61–70. DOI: 10.1038/nature11412 [PubMed: 23000897]

18. Wiener JR, et al. Overexpression of the protein tyrosine phosphatase PTP1B in human breast cancer: association with p185c-erbB-2 protein expression. Journal of the National Cancer Institute. 1994; 86:372–378. [PubMed: 7905928]

19. Bentires-Alj M, Neel BG. Protein-tyrosine phosphatase 1B is required for HER2/Neu-induced breast cancer. Cancer Res. 2007; 67:2420–2424. [PubMed: 17347513]

20. Julien SG, et al. Protein tyrosine phosphatase 1B deficiency or inhibition delays ErbB2-induced mammary tumorigenesis and protects from lung metastasis. Nature genetics. 2007; 39:338–346. [PubMed: 17259984]

21. Kim JS. Moyamoya Disease: Epidemiology, Clinical Features, and Diagnosis. Journal of stroke. 2016; 18:2–11. DOI: 10.5853/jos.2015.01627 [PubMed: 26846755]

22. Krishnan N, et al. Targeting the disordered C terminus of PTP1B with an allosteric inhibitor. Nature chemical biology. 2014; 10:558–566. DOI: 10.1038/nchembio.1528 [PubMed: 24845231]

23. Balavenkatraman KK, et al. Epithelial protein-tyrosine phosphatase 1B contributes to the induction of mammary tumors by HER2/Neu but is not essential for tumor maintenance. Molecular cancer research: MCR. 2011; 9:1377–1384. DOI: 10.1158/1541-7786.MCR-11-0198 [PubMed: 21849469]

24. Wiesmann C, et al. Allosteric inhibition of protein tyrosine phosphatase 1B. Nature structural & molecular biology. 2004; 11:730–737. DOI: 10.1038/nsmb803

25. Anso E, et al. Metabolic changes in cancer cells upon suppression of MYC. Cancer & metabolism. 2013; 1:7.doi: 10.1186/2049-3002-1-7 [PubMed: 24280108]

26. McDonough MA, et al. Selective inhibition of factor inhibiting hypoxia-inducible factor. Journal of the American Chemical Society. 2005; 127:7680–7681. DOI: 10.1021/ja050841b [PubMed: 15913349]

27. Chowdhury R, et al. Selective small molecule probes for the hypoxia inducible factor (HIF) prolyl hydroxylases. ACS chemical biology. 2013; 8:1488–1496. DOI: 10.1021/cb400088q [PubMed: 23683440]

28. Yan L, Colandrea VJ, Hale JJ. Prolyl hydroxylase domain-containing protein inhibitors as stabilizers of hypoxia-inducible factor: small molecule-based therapeutics for anemia. Expert opinion on therapeutic patents. 2010; 20:1219–1245. DOI: 10.1517/13543776.2010.510836 [PubMed: 20698812]

29. Tiganis T, Bennett AM. Protein tyrosine phosphatase function: the substrate perspective. The Biochemical journal. 2007; 402:1–15. DOI: 10.1042/BJ20061548 [PubMed: 17238862]

30. Flint AJ, Tiganis T, Barford D, Tonks NK. Development of "substrate-trapping" mutants to identify physiological substrates of protein tyrosine phosphatases. Proceedings of the National Academy of Sciences of the United States of America. 1997; 94:1680–1685. [PubMed: 9050838]

31. Gentile A, et al. Met-driven invasive growth involves transcriptional regulation of Arhgap12. Oncogene. 2008; 27:5590–5598. DOI: 10.1038/onc.2008.173 [PubMed: 18504429]

32. Mertins P, et al. Investigation of protein-tyrosine phosphatase 1B function by quantitative proteomics. Molecular & cellular proteomics: MCP. 2008; 7:1763–1777. DOI: 10.1074/mcp.M800196-MCP200 [PubMed: 18515860]

33. Liu W, et al. Identification of RNF213 as a susceptibility gene for moyamoya disease and its possible role in vascular development. PloS one. 2011; 6:e22542.doi: 10.1371/journal.pone.0022542 [PubMed: 21799892]

34. Kim W, et al. Systematic and quantitative assessment of the ubiquitin-modified proteome. Molecular cell. 2011; 44:325–340. DOI: 10.1016/j.molcel.2011.08.025 [PubMed: 21906983]

35. Weinberg DG, et al. Moyamoya disease: a review of histopathology, biochemistry, and genetics. Neurosurgical focus. 2011; 30:E20.doi: 10.3171/2011.3.FOCUS1151 [PubMed: 21631222]

36. Lutterman J, Scott M, Nass R, Geva T. Moyamoya syndrome associated with congenital heart disease. Pediatrics. 1998; 101:57–60. [PubMed: 9417151]

37. Comprehensive molecular characterization of human colon and rectal cancer. Nature. 2012; 487:330–337. DOI: 10.1038/nature11252 [PubMed: 22810696]

38. Wiesmann C, et al. Allosteric inhibition of protein tyrosine phosphatase 1B. Nature structural & molecular biology. 2004; 11:730–737. DOI: 10.1038/nsmb803

39. Liu W, et al. Identification of RNF213 as a susceptibility gene for moyamoya disease and its possible role in vascular development. PloS one. 2011; 6:e22542.doi: 10.1371/journal.pone.0022542 [PubMed: 21799892]

40. Ingber D, et al. Synthetic analogues of fumagillin that inhibit angiogenesis and suppress tumour growth. Nature. 1990; 348:555–557. DOI: 10.1038/348555a0 [PubMed: 1701033]

41. Bentires-Alj M, Neel BG. Protein-tyrosine phosphatase 1B is required for HER2/Neu-induced breast cancer. Cancer Res. 2007; 67:2420–2424. [PubMed: 17347513]

42. Ran FA, et al. Genome engineering using the CRISPR-Cas9 system. Nature protocols. 2013; 8:2281–2308. DOI: 10.1038/nprot.2013.143 [PubMed: 24157548]

43. van den Beucken T, et al. Hypoxia-induced expression of carbonic anhydrase 9 is dependent on the unfolded protein response. The Journal of biological chemistry. 2009; 284:24204–24212. DOI: 10.1074/jbc.M109.006510 [PubMed: 19564335]

44. Abdel Rahman AM, Ryczko M, Pawling J, Dennis JW. Probing the hexosamine biosynthetic pathway in human tumor cells by multitargeted tandem mass spectrometry. ACS chemical biology. 2013; 8:2053–2062. DOI: 10.1021/cb4004173 [PubMed: 23875632]

45. Abdel Rahman AM, et al. Golgi N-glycan branching N-acetylglucosaminyltransferases I, V and VI promote nutrient uptake and metabolism. Glycobiology. 2015; 25:225–240. DOI: 10.1093/glycob/cwu105 [PubMed: 25395405]

46. Abdel Rahman AM, Pawling J, Ryczko M, Caudy AA, Dennis JW. Targeted metabolomics in cultured cells and tissues by mass spectrometry: method development and validation. Analytica chimica acta. 2014; 845:53–61. DOI: 10.1016/j.aca.2014.06.012 [PubMed: 25201272]

47. Wu X, et al. Increased BRAF heterodimerization is the common pathogenic mechanism for noonan syndrome-associated RAF1 mutants. Molecular and cellular biology. 2012; 32:3872–3890. DOI: 10.1128/MCB.00751-12 [PubMed: 22826437]

48. Gross S, et al. Cancer-associated metabolite 2-hydroxyglutarate accumulates in acute myelogenous leukemia with isocitrate dehydrogenase 1 and 2 mutations. The Journal of experimental medicine. 2010; 207:339–344. DOI: 10.1084/jem.20092506 [PubMed: 20142433]

49. Ward PS, et al. The common feature of leukemia-associated IDH1 and IDH2 mutations is a neomorphic enzyme activity converting alpha-ketoglutarate to 2-hydroxyglutarate. Cancer cell. 2010; 17:225–234. DOI: 10.1016/j.ccr.2010.01.020 [PubMed: 20171147]

50. Sinha A, Ignatchenko V, Ignatchenko A, Mejia-Guerrero S, Kislinger T. In-depth proteomic analyses of ovarian cancer cell line exosomes reveals differential enrichment of functional categories compared to the NCI 60 proteome. Biochemical and biophysical research communications. 2014; 445:694–701. DOI: 10.1016/j.bbrc.2013.12.070 [PubMed: 24434149]

51. Cox J, Mann M. MaxQuant enables high peptide identification rates, individualized p.p.b.-range mass accuracies and proteome-wide protein quantification. Nature biotechnology. 2008; 26:1367–1372. DOI: 10.1038/nbt.1511

52. Udeshi ND, et al. Methods for quantification of in vivo changes in protein ubiquitination following proteasome and deubiquitinase inhibition. Molecular & cellular proteomics: MCP. 2012; 11:148–159. DOI: 10.1074/mcp.M111.016857 [PubMed: 22505724]

53. Thompson A, et al. Tandem mass tags: a novel quantification strategy for comparative analysis of complex protein mixtures by MS/MS. Analytical chemistry. 2003; 75:1895–1904. [PubMed: 12713048]

54. Senko MW, et al. Novel parallelized quadrupole/linear ion trap/Orbitrap tribrid mass spectrometer improving proteome coverage and peptide identification rates. Analytical chemistry. 2013; 85:11710–11714. DOI: 10.1021/ac403115c [PubMed: 24251866]

55. Ting L, Rad R, Gygi SP, Haas W. MS3 eliminates ratio distortion in isobaric multiplexed quantitative proteomics. Nature methods. 2011; 8:937–940. DOI: 10.1038/nmeth.1714 [PubMed: 21963607]

56. McAlister GC, et al. MultiNotch MS3 enables accurate, sensitive, and multiplexed detection of differential expression across cancer cell line proteomes. Analytical chemistry. 2014; 86:7150–7158. DOI: 10.1021/ac502040v [PubMed: 24927332]

57. Eng JK, McCormack AL, Yates JR. An approach to correlate tandem mass spectral data of peptides with amino acid sequences in a protein database. Journal of the American Society for Mass Spectrometry. 1994; 5:976–989. DOI: 10.1016/1044-0305(94)80016-2 [PubMed: 24226387]

58. Elias JE, Gygi SP. Target-decoy search strategy for increased confidence in large-scale protein identifications by mass spectrometry. Nature methods. 2007; 4:207–214. DOI: 10.1038/nmeth1019 [PubMed: 17327847]

59. Huttlin EL, et al. A tissue-specific atlas of mouse protein phosphorylation and expression. Cell. 2010; 143:1174–1189. DOI: 10.1016/j.cell.2010.12.001 [PubMed: 21183079]

60. Shannon P, et al. Cytoscape: a software environment for integrated models of biomolecular interaction networks. Genome Res. 2003; 13:2498–2504. DOI: 10.1101/gr.1239303 [PubMed: 14597658]

61. Maere S, Heymans K, Kuiper M. BiNGO: a Cytoscape plugin to assess overrepresentation of gene ontology categories in biological networks. Bioinformatics. 2005; 21:3448–3449. DOI: 10.1093/ bioinformatics/bti551 [PubMed: 15972284]

62. Sherman BT, et al. DAVID Knowledgebase: a gene-centered database integrating heterogeneous gene annotation resources to facilitate high-throughput gene functional analysis. BMC bioinformatics. 2007; 8:426.doi: 10.1186/1471-2105-8-426 [PubMed: 17980028]
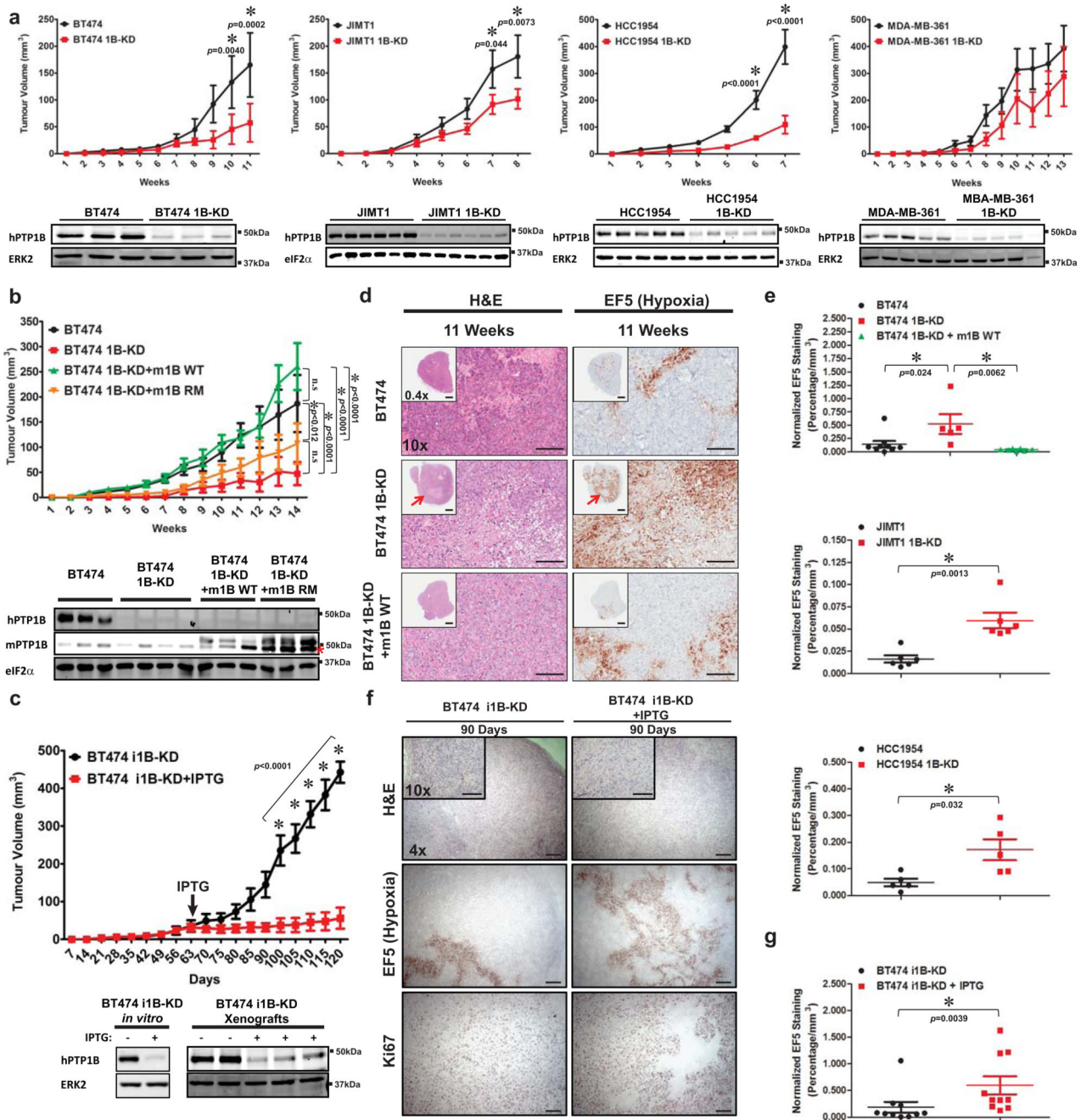
Figure 1.

Increased hypoxia and necrosis in PTP1B-deficient *HER2+* breast tumours. **a,** Tumour growth from Control and 1B-KD *HER2+* breast cancer cells injected subcutaneously into athymic nude mice. Independent mice were injected at the beginning of the experiment (*n=10* biologically independent xenografts for all groups except MDA-MB-361 1B-KD, where *n=8*). Tumours were collected during the experiment for histology and IHC, leaving *n=5* for the BT474 group at week 9-11, *n=8* for the HCC1954 group at week 5-7, and MDA-MB-361 (*n=9*) and MDA-MB-361 1B-KD (*n=7*) at week 11-13. **b,** Tumour growth from

mice injected with BT474 (*n=10*), BT474 1B-KD (*n=7*), BT474 1B-KD + m*Ptpn1* WT (*n=9*) or BT74 1B-KD + m*Ptpn1* RM (*n=10*) cells. All "n" values represent biologically independent xenografts. **c**, BT474 cells expressing IPTG-inducible *PTPN1* shRNA (i1B-KD) were allowed to form small tumours. IPTG was added to drinking water of half of the mice (*n=5* biologically independent xenografts). Immunoblots in **a**-**c** show PTP1B levels in individual tumours at the endpoint of each experiment; ERK2 or eIF2α are loading controls. Note the non-specific band (*) on the mPTP1B immunoblot in **b**. **d**, Representative sections from BT474 xenografts (from **b**) at 11 weeks post-injection, stained with H&E or EF5 (hypoxia). Insets and main images represent 0.4x or 10x magnifications, respectively. Red arrows indicate necrosis. **e**, EF5 staining area, normalized to tumour size, from BT474 (*n=9*), BT474 1B-KD (*n=6*), BT474 1B-KD + *mPtpn1* WT (*n=9*), JIMT1 (*n=6*), JIMT1 1B-KD (*n=6*), HCC1954 (*n=5*) and HCC1954 1B-KD (*n=5*) xenografts (from **a** and **b**). **f,**Representative Ki67- or EF-stained sections (from **c**) at 90 days post-injection. **g,** EF5 staining area, normalized to tumour size, from BT474 i1B-KD tumours after 28 days treatment with or without IPTG. Each point (total *n=10* per condition) represents one section from a biologically independent xenograft. Scale bars for 0.4x magnifications represent 1 mm, whereas they represent 250 μm for the 4x and 10x magnifications. Tumour growth curves and graphs (mean ± s.e.m.) were compared by two-tailed student *t*-test (**e, g**), one-way ANOVA (**e**) or two-way ANOVA (**a-c**), followed by Bonferroni post-hoc test.

Figure 2.
PTP1B-deficiency sensitizes *HER2*+ BC cells to hypoxia *in vitro*. **a,** Survival of Control and 1B-KD *HER2*+ BC cells in 0.1% O_2. Data shown represent mean values from three independent experiments; also see Supplementary Table 8). **b,** Colony formation by Control and 1B-KD *HER2*+ BC cells exposed for 24hrs to normoxia (21% O_2) or hypoxia (0.2% O_2) and then re-plated at the indicated cell numbers. Data are derived from one experiment with nine technical replicates. See Supplementary Table 8 for raw data. **c,** Survival in hypoxia (0.1% O_2) of Control and 1B-KD BT474 and SKBR3 cells or cells expressing WT *mPtpn1* cDNA or a phosphatase-impaired mutant (RM)**.**Data shown represent mean values from three (BT474-derived lines) or four (SKBR3-derived lines) biologically independent experiments (also see Supplementary Table 8). **d,** Effect of an allosteric PTP1B inhibitor (PTP Inhibitor XXII) on parental *HER2*+ BC cancer cells maintained in normoxia (21% O_2) or hypoxia (0.1% O_2). Cells were counted after 24 (HCC1954 (*n=5* for each group) and SKBR3 (*n=3* for each group)) or 48 (BT474 and MDA-MB-361 (*n=4* for each group and cell line) hour exposure to 0.1% O_2, and mean values are shown. For each line, "*n*" represents the number of biologically independent experiments (also see Supplementary

Table 8). Graphs represent mean ± s.e.m. and were compared by two-way (**a-c**) or one-way (**d**) ANOVA, followed by Bonferroni post-hoc test.
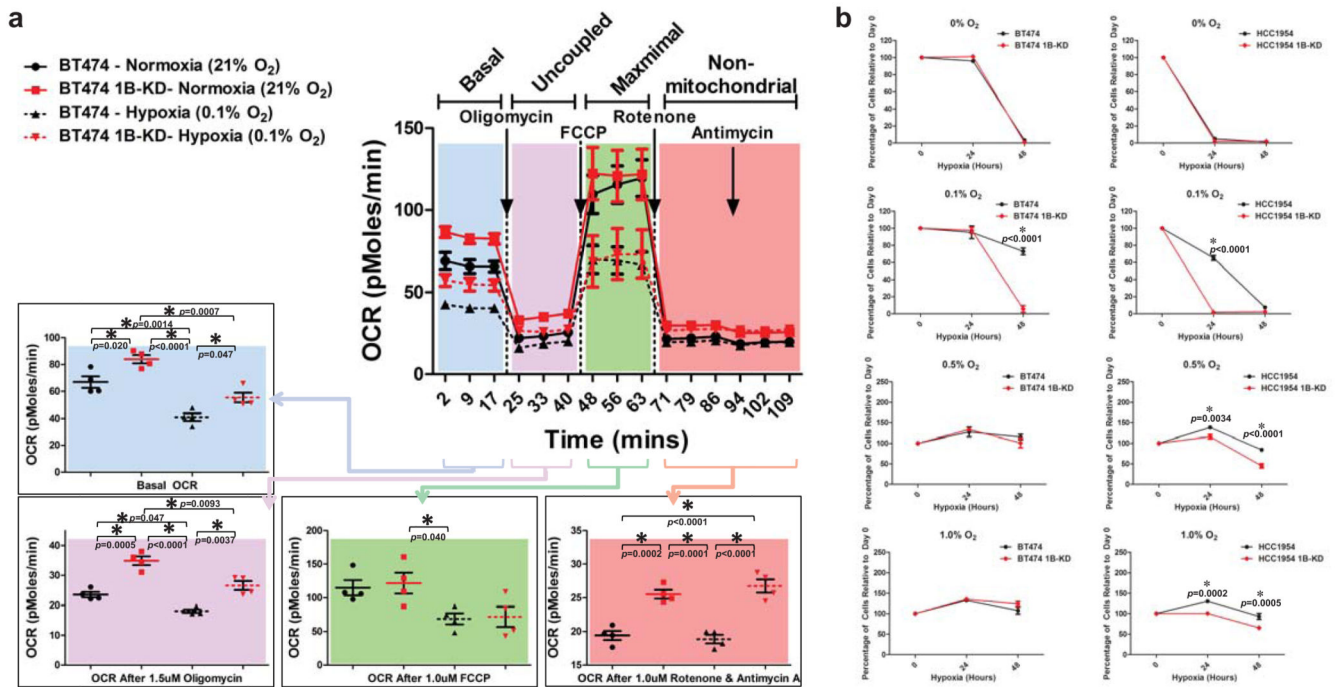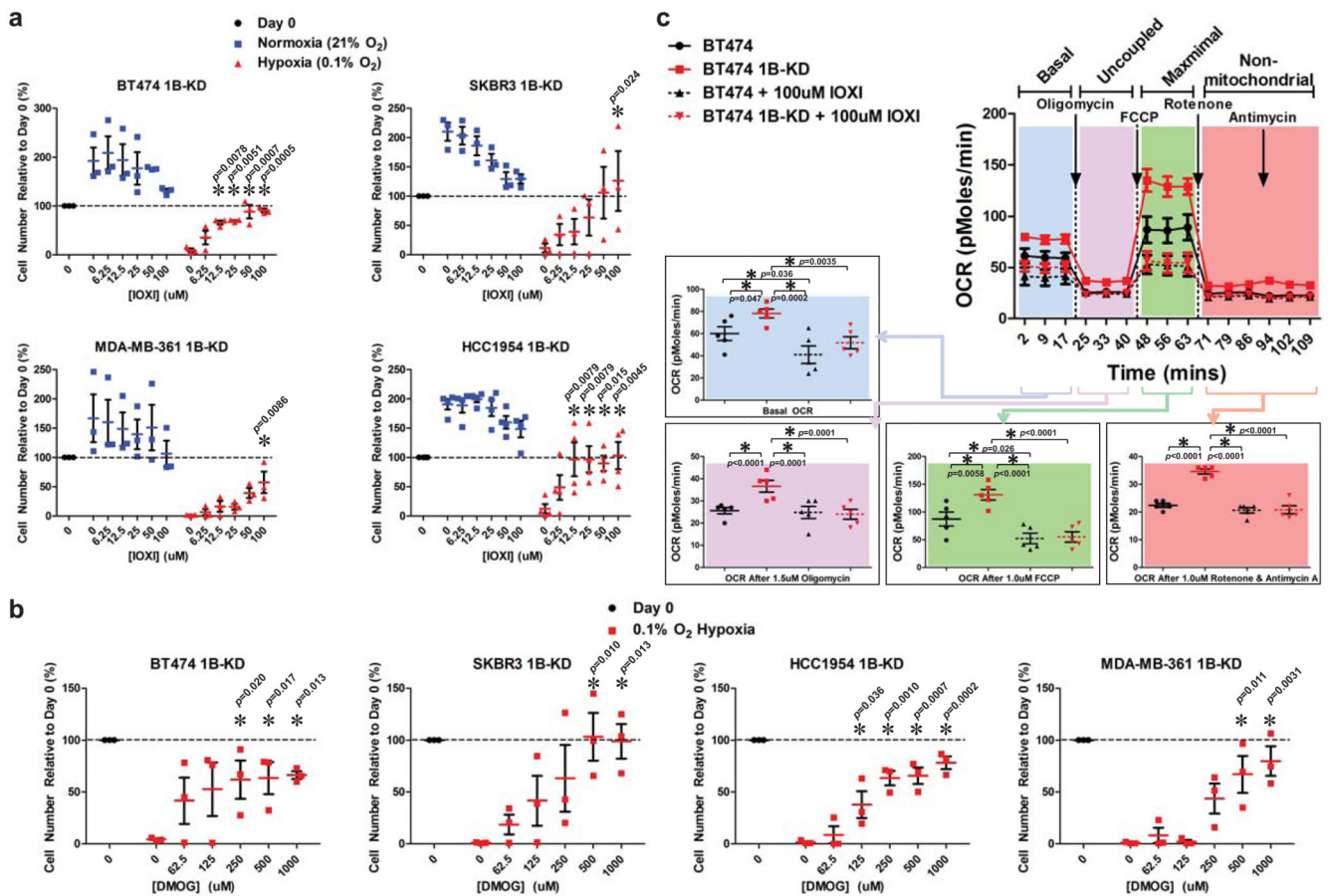
Figure 3.
PTP1B-deficient BC cells die due to increased non-mitochondrial oxygen consumption. **a**, Oxygen consumption rate (OCR) in Control and 1B-KD BT474 cells after exposure to normoxia (21% O_2) or hypoxia (0.1% O_2) for 24h. Oligomycin inhibits coupled respiration; FCCP was added to measure maximal respiration; Rotenone & Antimycin A block electron transport, enabling measurement of non-mitochondrial oxygen consumption (*n=4* biologically independent experiments for each group and condition; also see Supplementary Table 8). **b**, Effect of oxygen concentration on PTP1B-deficient *HER2+* BC cells. Survival of Control and 1B-KD BT474 and HCC1954 cells in anoxia (0%) or at the indicated O_2 concentrations (*n=3* biologically independent experiments for each group and condition; also see Supplementary Table 8)). Graphs represent mean ± s.e.m., and were compared using One-way (**a**) or two-way ANOVA (**b**), followed by Bonferroni post-hoc test.
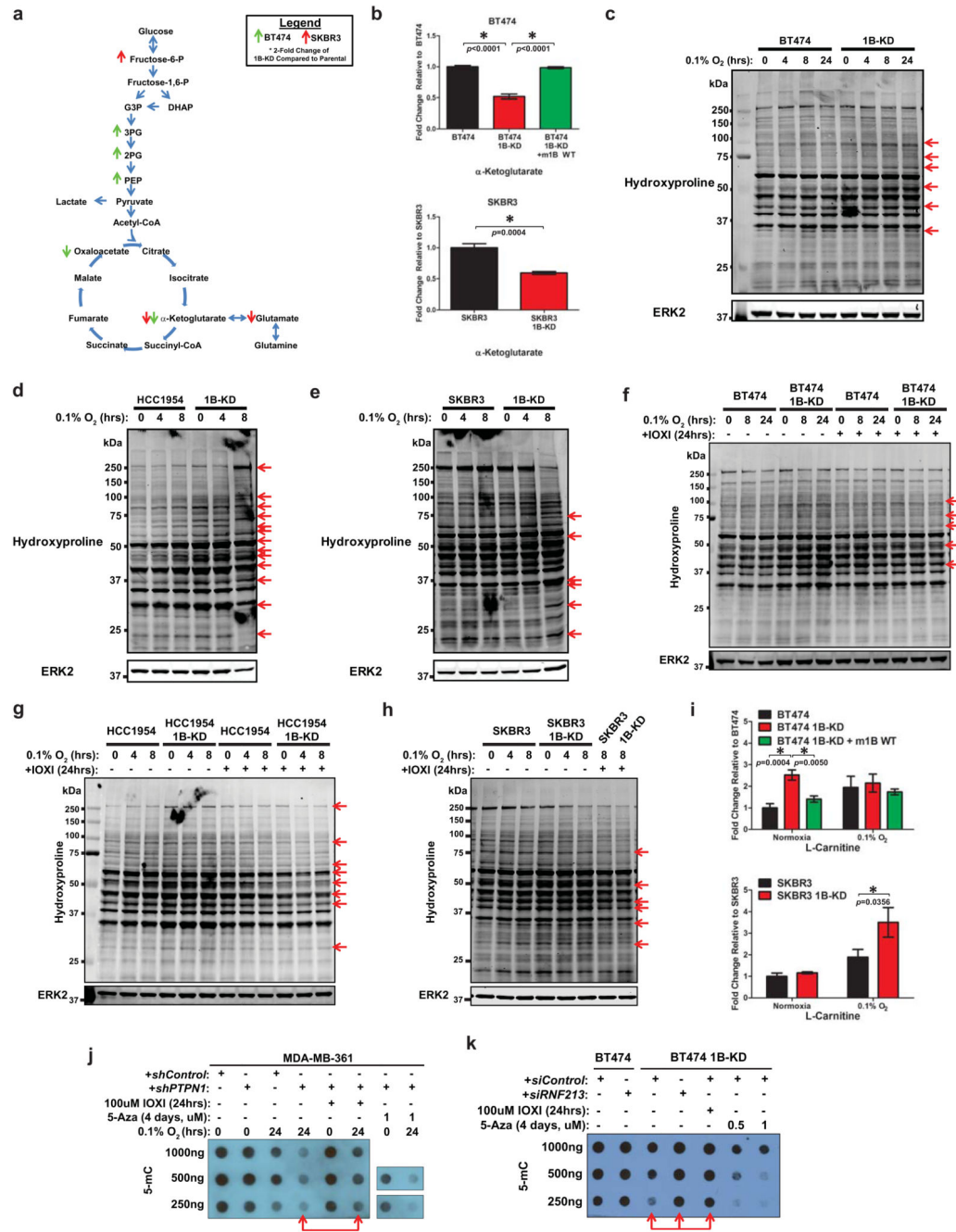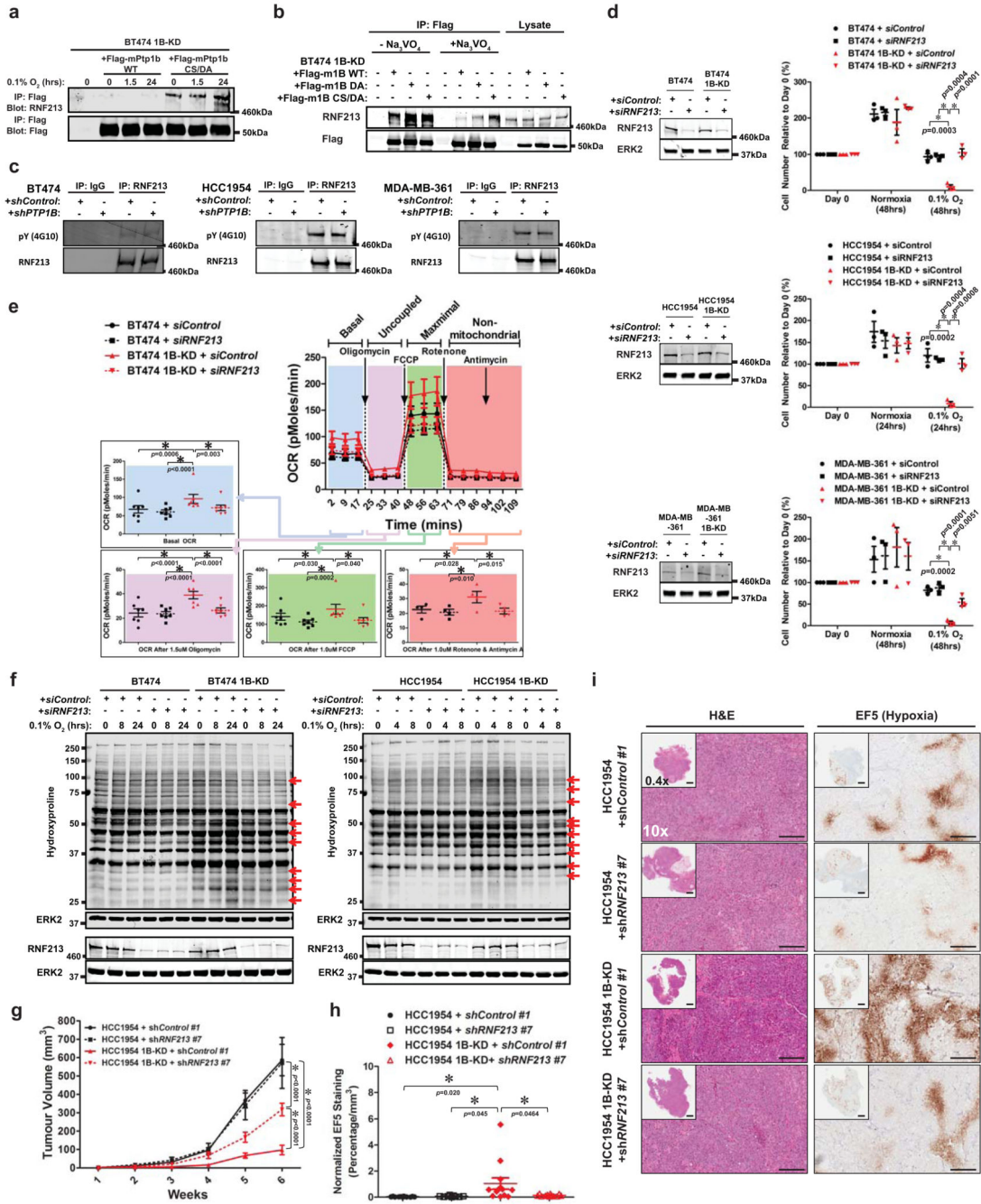
Figure 4.
PTP1B-deficiency activates multiple α-ketoglutarate dioxygenases. **a**, Schematic showing differences in glycolytic and TCA metabolites in Control and 1B-KD BT474 and SKBR3 cells under normoxia; also see Supplementary Figure 6 and Supplementary Table 1. **b**, Levels of α-ketoglutarate in parental and 1B-KD BT474 and SKBR3 cells under normoxia; note that the effects of 1B depletion in BT474 cells are rescued by mPTP1B expression (*n=5* biologically independent experiments for each group and condition). **c-e**, PTP1B-deficient *HER2*^{+} BC cells have global increase in hydroxylproline-containing proteins, consistent

with enhanced α-KG dioxygenase activity. Anti-hydroxyproline immunoblots of Control and 1B-KD *HER2⁺* BC cells exposed to 0.1% O₂ hypoxia for the indicated times. **f-h,** Similar experiments as in **c-e**, but 100μM IOXI was used to assess α-KG-dioxygenase dependency of bands. Red arrows indicate differences in band intensities. ERK2 serves as a loading control. **i,** Carnitine levels in parental and PTP1B-deficient BT474 and SKBR3 cells as determined by LC-MS/MS (*n=5* biologically independent experiments for each group and condition for each group, Supplementary Table 1) **j & k**, Reactivity of anti-5-methylcytosine (5-mC) antibodies with genomic DNA isolated from Control and 1B-KD MDA-MB-361 and BT474 cells in normoxia and/or hypoxia (as indicated), treated with or without IOXI. In **k**, BT474 cells were transfected with *siControl* or *siRNF213*, as indicated. 5-azacytidine was used as a positive control to block DNA methylation. Red arrows show that PTP1B-deficiency decreases anti-5 mC antibody reactivity, which is restored by IOXI treatment and/or *RNF213*-KD. Graphs (mean ± s.e.m.) were compared by one-tailed student t-test (i), two-tailed student *t*-test (b) or one-way ANOVA, followed by Bonferroni post-hoc test (b, i).
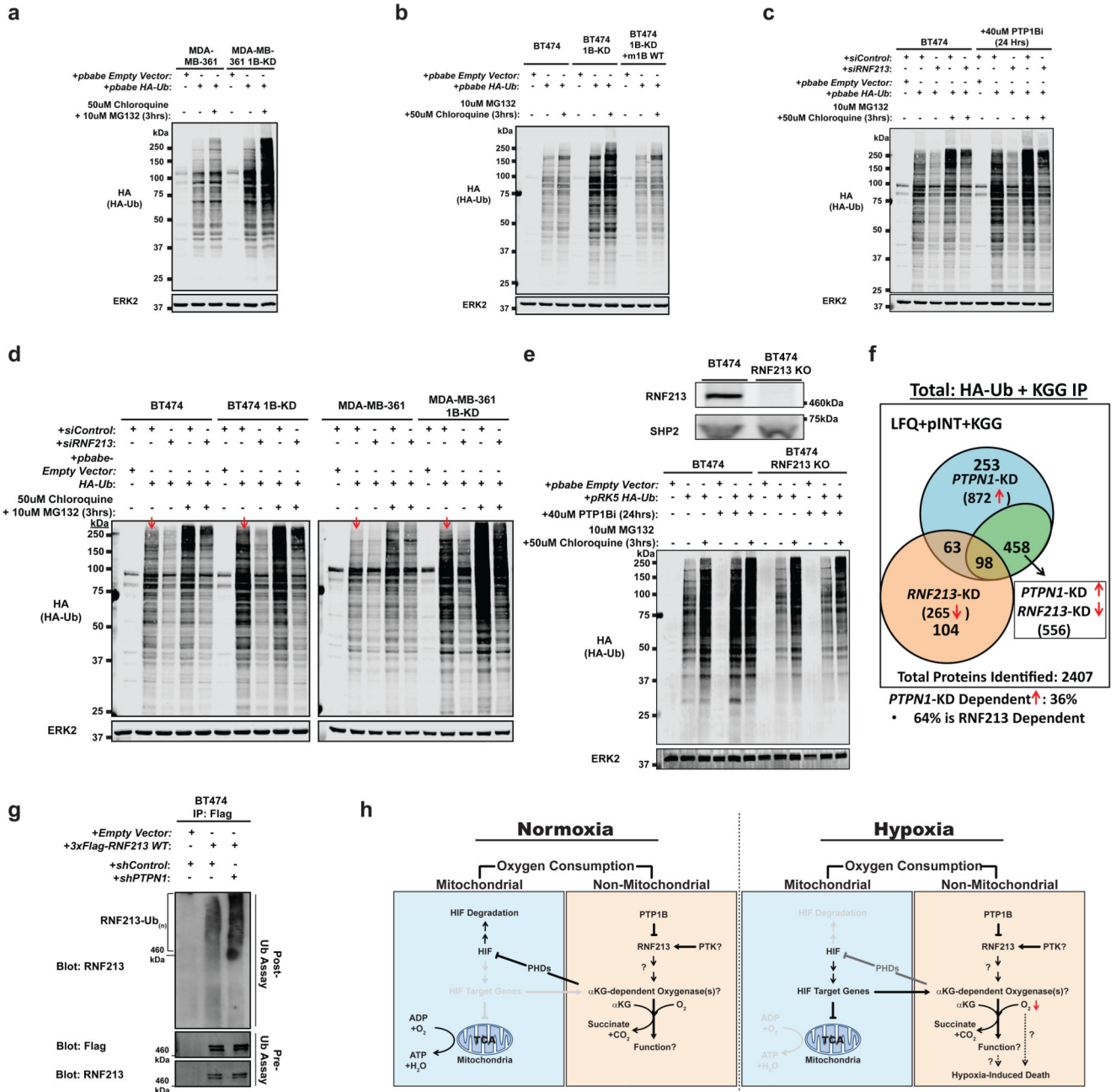
Figure 5.
Generic αKG-dependent dioxygenase inhibitors normalize hypoxia hypersensitivity and non-mitochondrial oxygen consumption in PTP1B-deficient BC cells. **a**, Effects of the generic αKG-dependent dioxygenase inhibitor IOXI on survival of 1B-KD *HER2+* BC cells in normoxia or hypoxia, as indicated. Cells were counted after 24 (HCC1954: *n=4* biologically independent experiments for each condition, and SKBR3: *n=3* biologically independent experiments for each condition) or 48 (BT474 and MDA-MB-361: *n=3* for each condition) hour exposure to 0.1% O_2 (also see Supplementary Table 8). **b**, Effect of generic αKG-dependent dioxygenase inhibitor DMOG on survival of the indicated Control and 1B-KD *HER2+* BC cells in hypoxia. Cells were counted after 24 (HCC1954 and SKBR3) or 48 (BT474 and MDA-MB-361) hour exposure to 0.1% O_2. Plots show mean ± s.e.m. from *n=3* biologically independent experiments for each condition (also see Supplementary Table 8). **c**, OCR of parental and 1B-KD BT474 cells with or without overnight exposure to IOXI (100μM) or the indicated mitochondrial inhibitors (*n=5* biologically independent experiments for each group and condition) All graphs represent mean ± s.e.m., and were compared by one-way ANOVA (**a-c**), followed by Bonferroni post-hoc test.

Figure 6.
RNF213 is a novel PTP1B substrate that regulates oxygen consumption and survival of
HER2^{+} BC cells in hypoxia. **a**, RNF213 immunoblot of PTP1B immunoprecipitates from
BT474 cells expressing Flag-mPtp1B WT or a substrate-trapping mutant (CS/DA). **b**,
Immunoblot showing co-immunoprecipitation of RNF213 and Flag-mPtp1B WT or the
indicated substrate trapping mutant (DA and CS/DA) in the absence or presence of the active
site tyrosine phosphatase inhibitor sodium orthovanadate (1mM). **c**, RNF213 is tyrosine
phosphorylated in *HER2*^{+} BC cells. Anti-phosphotyrosine immunoblots of RNF213

immunoprecipitates from Control and 1B-KD *HER2$^+$* BC cells. Note that RNF213 is tyrosine phosphorylated, although its overall level of phosphorylation is similar in both lines. **d**, *RNF213*-knockdown protects 1B-KD *HER2$^+$* BC cells from hypoxia-induced death (*n=3* biologically independent experiments for each group and condition; also see Supplementary Table 8). Cells were counted after 24 (HCC1954) or 48 (BT474 and MDA-MB-361) hour exposure to 0.1% O_2. Immunoblots show substantial depletion of RNF213 72hr post-transfection with RNF213 siRNAs in normoxia, compared with Control siRNAs. **e**, *RNF213*-knockdown normalizes increased oxygen consumption in BT474 1B-KD cells (*n=7* biologically independent experiments for each group in basal, uncoupled and maximal OCR; *n=4* biologically independent experiments for non-mitochondrial OCR; also see Supplementary Table 8). **f,** *RNF213*-knockdown normalizes levels of hydroxyproline-containing proteins in 1B-KD *HER2$^+$* BC cells. Hydroxyproline bands in Control and 1B-KD *HER2$^+$* BC cells after exposure to 0.1% O_2 for the indicated times are indicated by red arrows. **g,** Growth of HCC1954 + *shControl #1* (*n=12*), HCC1954 + *shRNF213 #7* (*n=9*), HCC1954 1B-KD + *shControl #1* (*n=12*), HCC1954 1B-KD + *shRNF213 #7* (*n=11*) tumours. **h**, EF5 staining area normalized to tumour size from HCC1954 + *shControl #1* (*n=12*), HCC1954 + *shRNF213 #7* (*n=9*), HCC1954 1B-KD + *shControl #1* (*n=13*), HCC1954 1B-KD + *shRNF213 #7* (*n=12*) tumours. **i**, Representative images of H&E and EF5 staining from Control and 1B-KD HCC1954 tumours expressing *shControl #1* or *shControl #7* (from **g**). All scale bars at 0.4x and 10x represent 1 mm or 250 μm, respectively. Graphs represent mean ± s.e.m., and were compared by one-way (**d**, **e**, **h**) or two-way (**g**) ANOVA, followed by Bonferroni post-hoc test.

Figure 7.
PTP1B-deficiency, via RNF213, alters the ubiquitylome in *HER2*+ BC cells. Immunoblot of HA-ubiquitin (HA-Ub) from transfected cells treated with or without proteasomal (MG132) and lysosomal (chloroquine) inhibitors for 3hrs, as indicated. Control and 1B-KD MDA-MB-361 cells (**a**), BT474 cells (**b**) or BT474 cells treated with PTP1B inhibitor for 24 hrs (**c**) are shown. **d**, Control and 1B-KD BT474 and MDA-MB-361 cells were transfected with an HA-Ub expression construct and the indicated siRNAs, treated with or without proteasomal (MG132) and lysosomal (chloroquine) inhibitors for 3 hrs in normoxia, and subjected to anti-HA immunoblotting. Red arrows indicate ubiquitylation in Control and 1B-

KD BT474 cells without proteasomal and lysosomal inhibitors. **e,** Parental BT474 and *RNF213*-KO cells were transfected with the HA-Ub expression construct, and treated with or without an allosteric PTP1B inhibitor, proteasomal and/or lysosomal inhibitor for the indicated times. Immunoblot shows lack of RNF213 in *RNF213-KO* BT474 cells generated by CRISPR/*Cas9* technology. SHP2 and ERK2 serve as loading controls. **f,** Venn diagram indicating the number of proteins that show 1.5-fold increased ubiquitylation upon *PTPN1*-KD alone, 0.67-fold decreased ubiquitylation upon *RNF213*-KD alone or that are affected by knockdown of *PTPN1* and *RNF213*, as determined by HA-Ub IP-MS and DiGly (KGG) enrichment. *PTPN1*-KD increased the ubiquitylation of ~40 % of the ubiquitylome, of which >60% were decreased by *RNF213*-KD. **g,** Auto-ubiquitylation activity of anti-Flag immunoprecipitates from Control and 1B-KD BT474 cells transfected with empty vector or 3xFlag-RNF213 WT under normoxic conditions. Anti-Flag and anti-RNF213 panels are loading controls **h,** Model for PTP1B regulation of tumour cell survival in hypoxia via RNF213. Active (black lines) and inactive (grey lines) pathways are shown during normoxia and hypoxia, as indicated. PTK: protein-tyrosine kinase; PHDs: prolyl-hydroxylase domain proteins; TCA: tricarboxylic acid cycle. See text for details.